

Three-Dimensional Anisotropic Noise Reduction with Automated Parameter Tuning: Application to Electron Cryotomography

J.J. Fernández^{1,2}, S. Li¹, and V. Lucic³

¹ MRC Laboratory of Molecular Biology, Hills Road, Cambridge CB2 2QH, UK

² Dept. Computer Architecture, University of Almería, Almería 04120, Spain
jjfdez@ual.es

³ Dept. Structural Biology, Max Planck Institute of Biochemistry, Martinsried, Germany

Abstract. This article presents an approach for noise filtering that is based on anisotropic nonlinear diffusion. The method combines edge-preserving noise reduction with a strategy to enhance local structures and a mechanism to further smooth the background. We have provided the method with an automatic mechanism for parameter self-tuning and for stopping the iterative filtering process. The performance of the approach is illustrated with its application to electron cryotomography (cryoET). CryoET has emerged as a leading imaging technique for visualizing the molecular architecture of complex biological specimens. A challenging computational task in this discipline is to increase the extremely low signal-to-noise ratio (SNR) to allow visualization and interpretation of the three-dimensional structures. The filtering method here proposed succeeds in substantially reducing the noise with excellent preservation of the structures.

1 Introduction

In many disciplines, raw data acquired from instruments are substantially corrupted by noise. Filtering techniques are then indispensable for a proper interpretation or post-processing. Standard linear filtering techniques based on local averages or Gaussian kernels succeed in reducing the noise, but at expenses of blurring edges and features. Nonlinear filtering techniques achieve better feature preservation as they try to adaptively tune the strength of the smoothing to the local structures found in the image.

Anisotropic nonlinear diffusion (AND) is currently one of the most powerful noise reduction techniques in the field of image processing and computer vision [1]. This technique takes into account the local structures found in the image to filter noise, preserve edges and enhance some features, thus considerably increasing the signal-to-noise ratio (SNR) with no significant quantitative distortions of the signal. Pioneered in 1990 by Perona and Malik [2], in the last decade AND has grown up to become a well-established tool for denoising multidimensional images [1,3,4,5,6].

Electron cryotomography (cryoET) has emerged as a leading imaging technique for structural analysis of large complex biological specimens at molecular resolution, which is critical to understand the cellular function [7]. CryoET allows the elucidation of the three-dimensional (3D) structure of specimens in their native state, but produces

extremely low contrast 3D density maps (known as “tomograms” in the field). The poor signal-to-noise ratio (SNR) that tomograms present, around 0.1, severely hinders their visualization and interpretation, and precludes the application of automatic image analysis techniques, such as segmentation or pattern recognition. Therefore sophisticated filtering techniques are indispensable for a proper interpretation of tomograms [6].

In this article an approach to anisotropic nonlinear filtering for cryoET is presented. The method combines structure-preserving noise reduction with a strategy for enhancement of planar and curvilinear local structures, and a mechanism to further filter the background. The method is provided with capability for automatic parameter tuning and for objectively stopping the iterative filtering process. We illustrate the method with its application to several 3D maps of biological specimens obtained by cryoET.

2 Review of Anisotropic Nonlinear Diffusion

AND accomplishes a sophisticated edge-preserving denoising that takes into account the structures at local scales. Conceptually speaking, AND tunes the strength of the smoothing along different directions based on the local structure estimated at every point of the multidimensional image.

2.1 Estimation of Local Structure

The *structure tensor* is the mathematical tool that allows us to estimate the local structure in a multidimensional image. The structure tensor of a 3D image I is a symmetric positive semi-definite matrix given by:

$$\mathbf{J}(I) = \begin{bmatrix} I_x^2 & I_x I_y & I_x I_z \\ I_x I_y & I_y^2 & I_y I_z \\ I_x I_z & I_y I_z & I_z^2 \end{bmatrix} \quad (1)$$

where $I_x = \frac{\partial I}{\partial x}$, $I_y = \frac{\partial I}{\partial y}$, $I_z = \frac{\partial I}{\partial z}$ are the derivatives of the image with respect to x , y and z , respectively. The components of \mathbf{J} are usually averaged with an Gaussian convolution kernel in order to represent the local structure at a higher scale.

The eigen-analysis of the structure tensor allows determination of the local structural features in the image [1]:

$$\mathbf{J}(I) = [\mathbf{v}_1 \ \mathbf{v}_2 \ \mathbf{v}_3] \cdot \begin{bmatrix} \mu_1 & 0 & 0 \\ 0 & \mu_2 & 0 \\ 0 & 0 & \mu_3 \end{bmatrix} \cdot [\mathbf{v}_1 \ \mathbf{v}_2 \ \mathbf{v}_3]^T \quad (2)$$

The orthogonal eigenvectors \mathbf{v}_1 , \mathbf{v}_2 , \mathbf{v}_3 provide the preferred local orientations, and the corresponding eigenvalues μ_1 , μ_2 , μ_3 (assume $\mu_1 \geq \mu_2 \geq \mu_3$) provide the average contrast along these directions. The first eigenvector \mathbf{v}_1 represents the direction of the maximum variance, whereas \mathbf{v}_3 points to the direction with the minimum variance. Based on the relative values of μ_i , basic local structures can be characterized (Fig. 1):

- Line-like structures have a preferred direction (\mathbf{v}_3) exhibiting a minimum variation whose eigenvalue is much lower than the other two, i.e. $\mu_1 \approx \mu_2 \gg \mu_3$. \mathbf{v}_1 and \mathbf{v}_2 are directions perpendicular to the line.

- Plane-like structures have two preferred directions exhibiting similar small contrast variation, whose eigenvalues are much lower than the first one, i.e. $\mu_1 \gg \mu_2 \approx \mu_3$. \mathbf{v}_1 represents the direction perpendicular to the plane-like structure, whereas \mathbf{v}_2 and \mathbf{v}_3 define the plane that better fits the local structure.
- Isotropic structures. When the two previous conditions do not hold, then the local structure is considered isotropic or unstructured. In general, for these structures, the eigenvalues have values of similar magnitude or order, i.e. $\mu_1 \approx \mu_2 \approx \mu_3$.

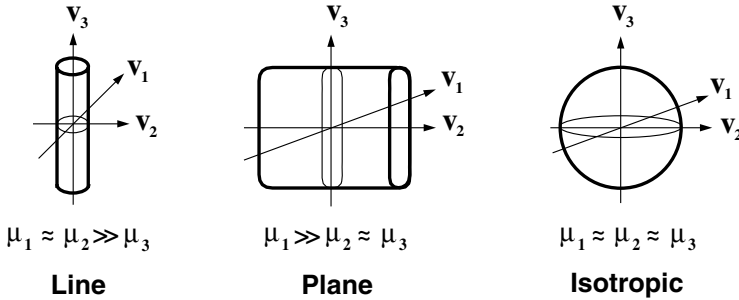


Fig. 1. Basic local structures found by eigen-analysis of the structure tensor. μ_1, μ_2, μ_3 are the eigenvalues. $\mathbf{v}_1, \mathbf{v}_2, \mathbf{v}_3$ are the corresponding eigenvectors.

2.2 Concept of Diffusion in Image Processing

Diffusion is a physical process that equilibrates concentration differences as a function of time, without creating or destroying mass. In image processing, density values play the role of concentration. This observation is expressed by the *diffusion equation* [1]:

$$I_t = \text{div}(\mathbf{D} \cdot \nabla I) \quad (3)$$

where $I_t = \frac{\partial I}{\partial t}$ denotes the derivative of the image I with respect to the time t , ∇I is the gradient vector, \mathbf{D} is a square matrix called *diffusion tensor* and div is the *divergence* operator.

The diffusion tensor \mathbf{D} allows us to tune the smoothing (both the strength and direction) across the image. \mathbf{D} is defined as a function of the structure tensor \mathbf{J} :

$$\mathbf{D} = [\mathbf{v}_1 \ \mathbf{v}_2 \ \mathbf{v}_3] \cdot \begin{bmatrix} \lambda_1 & 0 & 0 \\ 0 & \lambda_2 & 0 \\ 0 & 0 & \lambda_3 \end{bmatrix} \cdot [\mathbf{v}_1 \ \mathbf{v}_2 \ \mathbf{v}_3]^T \quad (4)$$

where \mathbf{v}_i denotes the eigenvectors of the structure tensor. The values of the eigenvalues λ_i define the strength of the smoothing along the direction of the corresponding eigenvector \mathbf{v}_i . The values of λ_i rank from 0 (no smoothing) to 1 (strong smoothing). In AND, the λ_i s are normally set up independently so that the smoothing is anisotropically adapted to the local structure of the image. Consequently, AND allows smoothing on the edges: Smoothing runs along the edges so that they are not only preserved but smoothed and enhanced. AND has turned out, by far, the most effective denoising method by its capabilities for structure preservation and feature enhancement [1,5,6].

2.3 Common Diffusion Approaches

AND may function differently, by either filtering noise or enhancing some structural features, depending on the definition of λ_i of the diffusion tensor \mathbf{D} . Currently, the most common ways of setting up \mathbf{D} give rise to the following diffusion approaches:

– EED: Edge Enhancing Diffusion.

The primary effects of EED are edge preservation and enhancement [1]. Here strong smoothing is applied along the direction corresponding to the minimum change (the third eigenvector, \mathbf{v}_3), while the strength of the smoothing along the other eigenvectors depends on the gradient: the higher the value is, the lower the smoothing strength is. The λ_i s are then set up as:

$$\begin{cases} \lambda_1 = g(|\nabla I|) \\ \lambda_2 = g(|\nabla I|) \\ \lambda_3 = 1 \end{cases} \quad (5)$$

with g being a monotonically decreasing function, such as [1]:

$$g(x) = 1 - \exp\left(\frac{-3.31488}{(x/K)^8}\right)$$

where $K > 0$ is a contrast threshold constant; Structures with $|\nabla I| > K$ are regarded as edges, otherwise as the interior of a region.

– CED: Coherence Enhancing Diffusion.

CED is able to connect interrupted lines and improve flow-like structures [3] and also enhance plane-like structures [6]. The strength of the smoothing along \mathbf{v}_2 must be tightly coupled to the plane-ness, given by $(\mu_1 - \mu_2)$, whereas the smoothing along \mathbf{v}_3 depends on the anisotropy $(\mu_1 - \mu_3)$. So, the λ_i s are then set up as:

$$\begin{cases} \lambda_1 \approx 0 \\ \lambda_2 = h(\mu_1 - \mu_2) \\ \lambda_3 = h(\mu_1 - \mu_3) \end{cases} \quad (6)$$

with h being a monotonically increasing function, such as [3]:

$$h(x) = \alpha + (1 - \alpha) \exp(-C/x^2)$$

where α is a regularization constant (typically 10^{-3}) and $C > 0$ is a threshold. Plane-like structures have $(\mu_1 - \mu_2)^2 > C$ and line-like ones have $(\mu_1 - \mu_3)^2 > C$.

3 Anisotropic Nonlinear Diffusion in cryoET

3.1 Diffusion Approach

In cryoET a hybrid diffusion approach is used in order to combine the advantages of both EED and CED simultaneously [5,8,6]. The strategy is based on the fact that the anisotropy $(\mu_1 - \mu_3)$ reflects the local relation of structure and noise. Therefore, we use this value as a switch: CED is applied if the anisotropy is larger than a suitably chosen threshold, otherwise EED is applied. The threshold t_{ec} is derived *ad hoc* as the maximum anisotropy found in a subvolume of the image containing only noise. This approach carries out an efficient denoising which highlights the edges and connects lines and enhances flow-like and plane-like structures.

3.2 Smoothing the Background with Gaussian Filtering

In our diffusion approach, we have included a strategy to further smooth out the background. Since the interesting structural features usually have higher density levels than the background, those voxels with density values below a threshold are considered as background, and hence linear Gaussian filtering is applied. The threshold t_g is computed from the average grey level in a subvolume of the tomogram that contains only noise, i.e. only background. As a consequence, those voxels that are considered background are significantly smoothed thanks to the Gaussian filtering.

3.3 Numerical Discretization of the Diffusion Equation

The diffusion equation, Eq. (3), can be numerically solved using finite differences. The term $I_t = \frac{\partial I}{\partial t}$ can be replaced by an Euler forward difference approximation. The resulting explicit scheme allows calculation of subsequent versions of the image iteratively:

$$I^{(k+1)} = I^{(k)} + \tau \cdot \left(\begin{aligned} &\frac{\partial}{\partial x}(D_{11}I_x) + \frac{\partial}{\partial x}(D_{12}I_y) + \frac{\partial}{\partial x}(D_{13}I_z) + \\ &\frac{\partial}{\partial y}(D_{21}I_x) + \frac{\partial}{\partial y}(D_{22}I_y) + \frac{\partial}{\partial y}(D_{23}I_z) + \\ &\frac{\partial}{\partial z}(D_{31}I_x) + \frac{\partial}{\partial z}(D_{32}I_y) + \frac{\partial}{\partial z}(D_{33}I_z) \end{aligned} \right) \quad (7)$$

where τ denotes the time step size, $I^{(k)}$ denotes the image at time $t_k = k\tau$ and the D_{mn} terms represent the components of the diffusion tensor \mathbf{D} .

In this work, we have approximated the spatial derivatives ($\frac{\partial}{\partial x}$, $\frac{\partial}{\partial y}$ and $\frac{\partial}{\partial z}$) by means of filters with optimally directional invariance due to their better capabilities for structural preservation [4,8]. This discretization scheme is much more stable [4] and allows up to four times larger time step size ($\tau = 0.4$) than the traditional explicit scheme based on central differences ($\tau = 0.1$). Our scheme may thus require up to 4 times less iterations to obtain similar improvement in SNR.

3.4 The Stopping Criterion: Noise Estimate Variance

AND works iteratively, yielding successive smoother versions of the image, gradually removing noise and details. The process should stop before the signal in the image is significantly affected. In this work, we use the *noise estimate variance* (NEV) stopping criterion [6]. Here, the noise that has been filtered at time t is estimated as the difference between the original noisy image, I^0 , and its current filtered version, I^t . The variance of this noise estimate increases monotonically from 0 to $\text{var}(I^0)$ during diffusion. The optimal stopping time is the time slot where $\text{var}(I^0 - I^t)$ reaches the variance of the noise subvolume in the original noisy image $\text{var}(I_N^0)$:

$$t_{\text{stop}} = \arg \min_t \{ |\text{var}(I_N^0) - \text{var}(I^0 - I^t)| \}$$

3.5 Automatic Parameter Tuning

The diffusion process is controlled by a number of parameters. Some of them are automatically tuned based on the statistics of a subvolume, extracted from the tomogram, that only contains noise: in particular, the NEV threshold $\text{var}(I_N^0)$, and the thresholds t_{ec} and t_g . However, setting up the parameters K and C controlling the EED and CED diffusion processes, respectively, is far from trivial [5,8,6]. So far, they were set up

manually based on the density range of the input tomogram, and they were fixed for the whole diffusion process [5,8,6]. In this work, we present a strategy to tune these parameters automatically based on the statistics of the noise subvolume previously mentioned. K and C can be set up as the average gradient and square anisotropy $(\mu_1 - \mu_3)^2$, respectively, found in the noise subvolume at each iteration. With this strategy, the parameters K and C do not keep fixed for the whole process any more. Instead, they evolve with iterations according to the noise and local structure remaining in the tomogram.

3.6 Scheme of Our Diffusion Approach

The outline of our AND approach is the following:

(0.) Compute NEV threshold from the subvolume containing noise.

It computes the threshold $\text{var}(I_N^0)$ used for the stopping criterion.

- $\text{var}(I_N^0)$ is the variance found in the noise subvolume.

(1.) Compute statistics of the subvolume containing noise.

Based on the statistics, it computes:

- the threshold t_{ec} used to switch between EED and CED.
 - t_{ec} is the maximum anisotropy $(\mu_1 - \mu_3)$ in the noise subvolume.
- the threshold t_g used to apply Gaussian filtering.
 - t_g is the average grey level in the noise subvolume.
- the parameter K used for EED.
 - K is the average gradient in the noise subvolume.
- the parameter C used to CED.
 - C is the average square anisotropy $(\mu_1 - \mu_3)^2$ in the noise subvolume.

(2.) Compute the structure tensor \mathbf{J} .

(3.) Compute the diffusion tensor \mathbf{D} .

For every voxel:

(3.1.) Analysis of the local structure.

It decides if the voxel is to be processed as EED, CED or background.

- The voxel is considered background if its grey level is lower than t_g .
- CED is to be applied, if the local anisotropy $(\mu_1 - \mu_3)$ is larger than t_{ec} .
- Otherwise, EED is to be applied.

(3.2.) Computation:

- Linear Diffusion.
 - If background, linear diffusion (i.e. Gaussian filtering) is applied.
- EED: Edge Enhancing Diffusion.
 - If EED, the diffusion tensor \mathbf{D} is computed according to Eqs. (4) and (5).
- CED: Coherence Enhancing Diffusion.
 - If CED, the diffusion tensor \mathbf{D} is computed according to Eqs. (4) and (6).

(4.) Solve the partial differential equation of diffusion, Eqs. (3) and (7).

(5.) Iterate: go to step (1.)

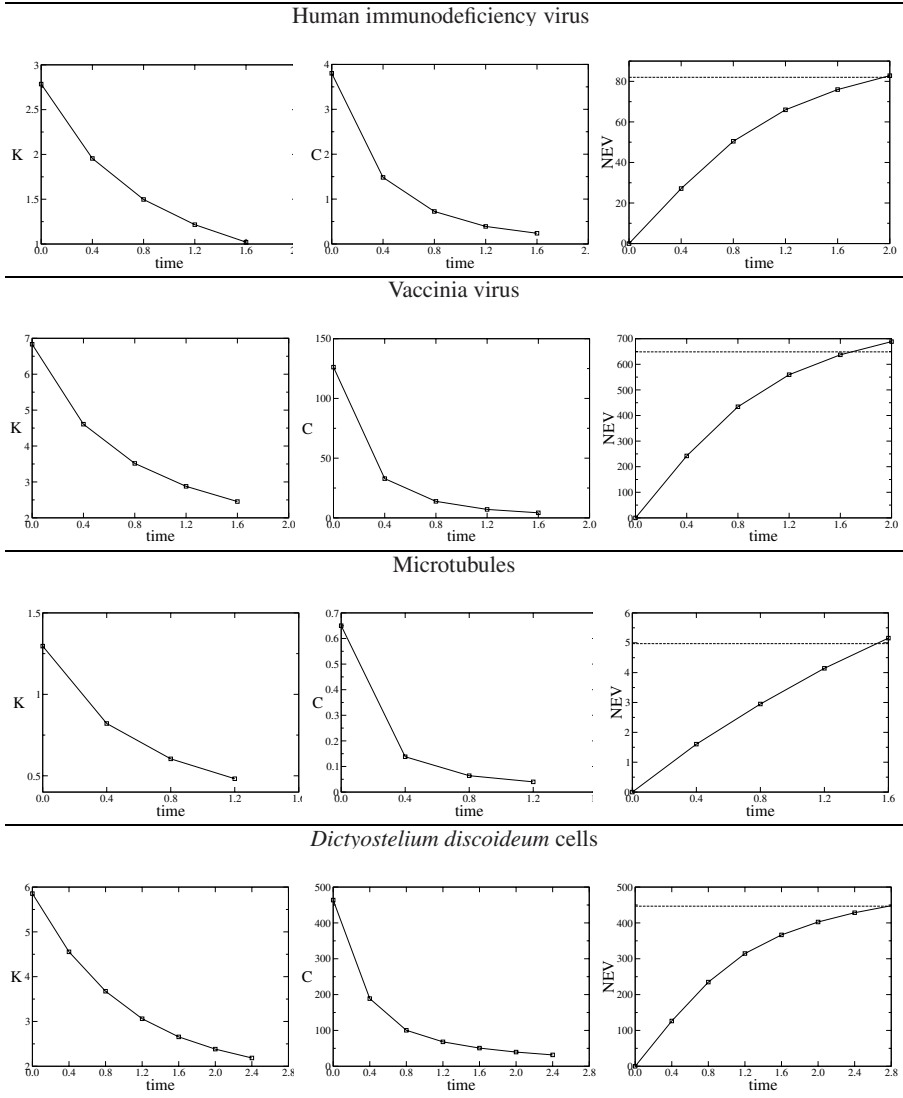
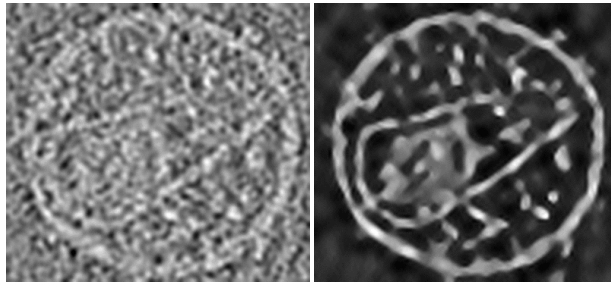


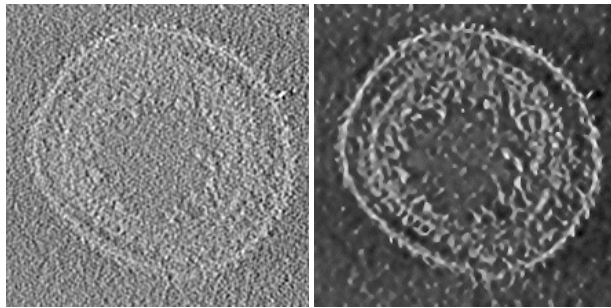
Fig. 2. Evolution of the denoising parameters with the iterations. The little squares in the graphs represents the values at the iterations, whereas X axis represents denoising time. The curves for K and C show the values used for the corresponding iteration. The NEV curve show the NEV measured at the corresponding iteration and the dashed-line represents the threshold to stop the process.

4 Experimental Applications

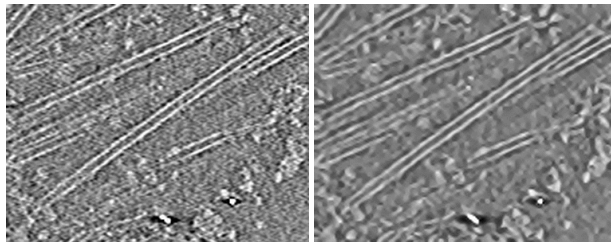
The AND approach presented here has been applied to tomograms of four different biological specimens: human immunodeficiency virus (HIV) [9], vaccinia virus (VV) [10], microtubules (MTs) [11] and *Dictyostelium discoideum* cells (DDC) [12].



Human immunodeficiency virus



Vaccinia virus



Microtubules

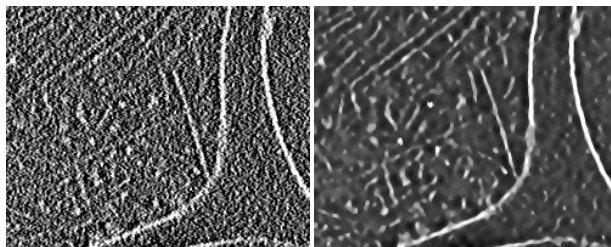
*Dictyostelium discoideum* cells

Fig. 3. Visual results from denoising. Left: a slice extracted from the original tomogram. Right: the same slice extracted from the denoised tomogram.

Fig. 2 shows the evolution of the denoising parameters during the iterative process for all the tomograms. The curves on the right show the evolution of the NEV and the iteration where the denoising process stopped because the NEV threshold (shown with dashed lines) was reached. For HIV, VV, MTs and DDC, the number of iterations used was 5, 5, 4, 7, respectively. These numbers of iterations correspond to a denoising time of 2.0, 2.0, 1.6 and 2.8, respectively, using a time step size of $\tau = 0.4$. In general, the NEV curves are logarithm-like, exhibiting a larger reduction of noise variance at the first iterations and becoming progressively smaller.

The evolution of K with the iterations, as seen in Fig. 2, shows a negative exponential-like curve. The fact that K is higher at the first iterations means that the strength of the smoothing is higher at the beginning and progressively decays down with the iterations. Furthermore, noise with high gradient (e.g. shot noise) is substantially smoothed at the beginning. Then, the denoising process gradually focuses on more homogeneous areas. This behaviour is consistent with the progressively smaller reduction of noise variance as seen in the NEV curves.

Fig. 2 shows that the evolution of C with the iterations also follows a negative exponential-like curve. The fact that C is higher at the first iterations means that the strength of the enhancement is lower at the beginning and progressively goes up as the iterations evolve. This behaviour reflects that the enhancement of the features increases gradually, as the local structures are reinforced with the iterations.

Fig. 3 shows visual results obtained from noise reduction applied to the tomograms of the different specimens. A single slice extracted from the 3D tomograms is shown. All the results clearly show significant noise reduction with excellent structure preservation. The structural features that are of interest from the biological point of view are smoothed and enhanced substantially thanks to the hybrid EED/CED diffusion process. In particular, the CED approach plays an essential role in the enhancement of the membranes and other linear and planar features of the specimens. The strategy to further smooth the background has a remarkable performance whereby the specimens' features are successfully highlighted over the background.

Fig. 3 clearly shows the benefits of denoising for interpretation of the biological structures. In the case of HIV, there is strong enhancement of the outer membrane and the core's surface, as well as some other bodies inside the core. In the case of VV, denoising has significantly improved planar features, allowing the interpretation of the architecture of the virus, e.g. the outer membrane and the core made up of a membrane and a palisade. With regard to the MTs, the continuity along them and their interactions are apparent. Finally, denoising has emphasized the membranes of the cell and the fibrous structures that compose the cell's cytoplasm in the DDC tomogram.

The ability to parameter self-tuning provided in the denoising method has allowed high levels of autonomy. Apart from the input tomogram and the coordinates of the noise subvolume used for parameter tuning, no other parameters were needed. This makes this method very appropriate for users non-expert in the details of denoising.

5 Conclusion

We have presented a method to perform structure-preserving denoising based on anisotropic nonlinear diffusion. The AND approach relies on a hybrid strategy that

combines noise reduction and feature enhancement. A strategy to further smooth out the background and highlight structural features has been included. We have provided a mechanism for automatic parameter tuning and for stopping the iterative denoising process. This anisotropic noise reduction method has been applied to CryoET, and the results show that it succeeds in filtering noise and emphasizing the features of interest. Therefore, this method facilitates interpretation of the structural information concealed in the noisy cryo-tomograms. The parameter self-tuning provided in the method allows high levels of autonomy and no user intervention required. This ability makes this method well suited for structural biologists working in cryoET, usually non-experts in AND.

Acknowledgments

The authors thank Dr. R.A Crowther for fruitful discussions; Drs. O. Medalia for the *D. discoideum* dataset; Drs. J.L. Carrascosa for the VV dataset. The HIV dataset was obtained from the EBI-MSD database. Work partially supported by the MRC and grants MEC-TIN2005-00447, EU-FP6-LSHG-CT-2004-502828, JA-P06-TIC1426.

References

1. Weickert, J.: Anisotropic Diffusion in Image Processing. Teubner (1998)
2. Perona, P., Malik, J.: Scale space and edge detection using anisotropic diffusion. *IEEE Trans. Patt. Anal. Mach. Intel.* 12, 629–639 (1990)
3. Weickert, J.: Coherence-enhancing diffusion filtering. *Int. J. Computer Vision* 31, 111–127 (1999)
4. Weickert, J., Scharr, H.: A scheme for coherence-enhancing diffusion filtering with optimized rotation invariance. *J. Visual Comm. Imag. Repres.* 13, 103–118 (2002)
5. Frangakis, A.S., Stoschek, A., Hegerl, R.: Wavelet transform filtering and nonlinear anisotropic diffusion assessed for signal reconstruction performance on multidimensional biomedical data. *IEEE Trans. BioMed. Engineering* 48, 213–222 (2001)
6. Fernandez, J.J., Li, S.: Anisotropic nonlinear filtering of cellular structures in cryo-electron tomography. *Computing in Science and Engineering* 7(5), 54–61 (2005)
7. Sali, A., Glaeser, R., Earnest, T., Baumeister, W.: From words to literature in structural proteomics. *Nature* 422, 216–225 (2003)
8. Fernandez, J.J., Li, S.: An improved algorithm for anisotropic nonlinear diffusion for denoising cryo-tomograms. *J. Struct. Biol.* 144, 152–161 (2003)
9. Briggs, J., Grunewald, K., Glass, B., Forster, F., Krausslich, H., Fuller, S.: The mechanism of HIV-1 core assembly: Insights from 3D reconstructions of authentic virions. *Structure* 14, 15–20 (2006)
10. Cyrklaff, M., Risco, C., Fernandez, J.J., Jimenez, M.V., Esteban, M., Baumeister, W., Carrascosa, J.L.: Cryo-electron tomography of vaccinia virus. *Proc. Natl. Acad. Sci. USA* 102, 2772–2777 (2005)
11. Hoog, J., Schwartz, C., Noon, A., O'Toole, E., Mastronarde, D., McIntosh, J., Antony, C.: Organization of interphase microtubules in fission yeast analyzed by electron tomography. *Dev. Cell* 12, 349–361 (2007)
12. Medalia, O., Weber, I., Frangakis, A.S., Nicastro, D., Gerisch, G., Baumeister, W.: Macromolecular architecture in eukaryotic cells visualized by cryoelectron tomography. *Science* 298, 1209–1213 (2002)